Near- and subbarrier elastic and quasielastic scattering of the weakly bound ^{6}Li projectile on ^{144}Sm

D. S. Monteiro,[1] O. A. Capurro,[2] A. Arazi,[2,3] J. O. Fernández Niello,[2,3,4] J. M. Figueira,[2,3] G. V. Martí,[2] D. Martínez Heimann,[2,3] A. E. Negri,[2,3] A. J. Pacheco,[2,3] V. Guimarães,[5] D. R. Otomar,[1] J. Lubian,[1] and P. R. S. Gomes[1,*]

[1]*Instituto de Física, Universidade Federal Fluminense, Av. Litoranea s/n, Gragoatá, Niterói, R.J., 24210-340, Brazil*

[2]*Laboratorio TANDAR, Comisión Nacional de Energía Atómica, Av. General Paz 1499, 1650 San Martín, Buenos Aires, Argentina*

[3]*CONICET, Av. Rivadavia 1917, Buenos Aires (1033), Argentina*

[4]*Escuela de Ciencia y Tecnología, Univ. Nac. de San Martín, San Martín (1650), Buenos Aires, Argentina*

[5]*Instituto de Física, Universidade de São Paulo, Caixa postal 66318, 05315-970, São Paulo, S.P., Brazil*

(Received 17 October 2008; published 5 January 2009)

High-precision data of backward-angle elastic and quasielastic scattering for the weakly bound ^{6}Li projectile on ^{144}Sm target at deep–sub-barrier, near-, and above-barrier energies were measured. From the deep–sub-barrier data, the surface diffuseness of the nuclear interacting potential was studied. Barrier distributions were extracted from the first derivatives of the elastic and quasielastic excitation functions. It is shown that sequential breakup through the first resonant state of the ^{6}Li is an important channel to be included in coupled-channels calculations, even at deep–sub-barrier energies.

DOI: 10.1103/PhysRevC.79.014601 PACS number(s): 25.70.Mn, 25.70.Bc, 24.10.Eq

I. INTRODUCTION

In the past several years, the influence of the breakup of weakly bound nuclei on the elastic scattering and other reaction channels has been widely studied [1]. This has been done, for example, through studies of barrier distributions derived from fusion measurements involving the weakly bound projectiles ^{6,7}Li, ^{9}Be on heavy targets [2–4]. Alternative representations of the barrier distributions can be obtained from quasi-elastic scattering (QES) and elastic-scattering excitation functions at backward angles, but so far they have been mostly used in the study of systems involving tightly bound projectiles.

Quasielastic scattering is defined as the sum of all direct mechanisms such as elastic- and inelastic-scattering, transfer, and breakup processes. Because fusion is connected with the transmission through a barrier and large-angle quasielastic scattering is related with the reflection at the barrier, owing to the conservation of the reaction flux, these two processes may be considered as complementary to each other. Therefore, information about the fusion process may be obtained from measurements of QES cross sections at backward angles, which in most situations is easier to explore experimentally.

The determination of the barrier distribution from fusion measurements is obtained by taking the second derivative of the corresponding excitation function [5]. Another representation of the barrier distribution can be deduced from the first derivative of the backward-angle quasi-elastic-scattering excitation function [6]

$$D_{\rm qel}(E) = -\frac{d}{dE}\left[\frac{d\sigma_{\rm qel}}{d\sigma_{\rm Ruth}}(E)\right], \qquad (1)$$

where $\sigma_{\rm Ruth}$ is the Rutherford cross section. Because in Eq. (1) only first derivatives are involved, the barrier distribution derived from QES data carries lower uncertainties than the one deduced from fusion measurements. Actually, it has been proven for different systems that the two representations of the barrier distribution are equivalent (e.g., Refs. [7–9]).

The barrier structure of reaction mechanisms can be also inferred from elastic-scattering excitation functions at backward angles through the expression

$$D_{\rm el}(E) = -\frac{d}{dE}\left[\sqrt{\frac{d\sigma_{\rm el}}{d\sigma_{\rm Ruth}}(E)}\right], \qquad (2)$$

although this representation can be less detailed than the previous ones [10].

Large-angle QES has been studied at deep–sub-barrier and near-barrier energies for a variety of systems. However, there is only one preliminary report [11] on the investigation of this process for systems involving weakly bound nuclei, where the breakup channel was included as one of the quasielastic processes. Following the projectile breakup channel different processes may occur: one of the fragments may fuse with the target in a process named incomplete fusion (ICF) or all the fragments may fly away from the target in a process called non–capture breakup (NCBU) [1]. Fusion of all the fragments with the target would lead to a sequential complete fusion (SCF), but this process is unlikely to occur. Therefore, for weakly bound systems, QES—now including NCBU and ICF—can be considered as the complementary part to the complete fusion (CF) of the projectile with the target.

It is worth mentioning that in most of the weakly bound systems it is very difficult to separate experimentally CF from ICF events, and hence only their sum, or total fusion, could be measured. Therefore, it is more convenient to use QES data to extract information on the effect of the projectile breakup on other reaction channels.

Moreover, additional information can be extracted from low-energy QES data. It has been recently shown [12,13] that high-precision backward-angle QES measurements at deep–sub-barrier energies allow one the determination of the surface diffuseness parameter of the interaction nucleus-nucleus

*paulogom@if.uff.br

potentials. At this energy regime, coupled-channels effects might be neglected, and therefore simple one-dimensional optical potentials could be used to derive the diffuseness parameter.

In the present article we report the measurement of large-angle elastic and inelastic cross sections for the ^{6}Li+^{144}Sm system, at deep–sub-barrier and near-barrier energies. Two representations of fusion barrier distribution are extracted from these data. In Sec. II of this article we present experimental details and results. In Sec. III we analyze the deep–sub-barrier QES data connected with the surface diffuseness of the interaction nucleus-nucleus potential. In Sec. IV we present the experimental excitation functions and barrier distributions and we compare these results with coupled-channels calculations to assess the influence of the breakup of the ^{6}Li on both the excitation function and the potential barrier distribution. Finally, in Sec. V we present a summary of the results and some conclusions.

II. EXPERIMENTAL DETAILS AND RESULTS

The experiments were performed at the Tandar Laboratory. Beams of ^{6}Li were delivered by the tandem accelerator at bombarding energies from 14 to 35 MeV (40% below and above the nominal Coulomb barrier). The beam energy was varied in steps of 1 MeV at values well below and well above the barrier, whereas a 0.5-MeV step was chosen at near-barrier energies. These energy steps proved to be fine enough to deduce barrier distributions from quasi-elastic-scattering excitation function. The terminal voltage was increased monotonically to reduce magnetic hysteresis effects [14]. A good stability of the accelerator ion source during the experiment allowed us to attribute the uncertainty in the beam energy to the aperture of the slits placed at the exit of the analyzing magnet (near 0.5% for a slits aperture of 10 mm). Beam currents ranged from 4 to 100 pnA. The irradiation time of each run at low bombarding energies was such that the number of events in the elastic peak was of the order of 10.000 (1% statistical uncertainty). However, due to very small quasielastic cross sections at backward angle for the highest energies, such a requirement was relaxed to a few hundred events. The ^{144}Sm target was isotopically enriched to 88%, its thickness was of 200 μg/cm^2, and it was evaporated onto a 20 μg/cm^2 carbon backing. We expect no significant effect due to the target impurities, because most of them come from ^{147,148,149}Sm and only 3% come from from the deformed ^{152,154}Sm.

The detection system consisted of two solid ΔE-E telescopes, with thicknesses of 15–150 and 30–150 μm, respectively. These detectors were placed at $\pm 170^{\circ}$ relative to the beam direction and the corresponding angular apertures were 1.7° and 1.3°, respectively. Two surface barrier silicon detectors were placed at $\pm 30.8^{\circ}$ relative to the beam direction and were used for normalization purposes (monitor detectors). The uncertainty in the angular positions of the telescopes and monitors are 0.1°. This precision could be checked by the results at deep–sub-barrier energies, for which the ratio elastic/Rutherford cross sections for the monitors were unitary, within the error bars. function was obtained by means of the

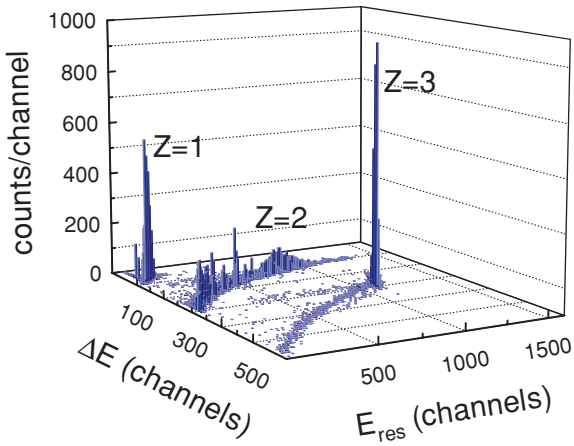

FIG. 1. (Color online) Bidimensional (ΔE-$E_{\rm res}$) spectrum obtained for the ^{6}Li + ^{144}Sm system at $E_{\rm lab} = 24.5$ MeV. The quasielastic to Rutherford scattering at backward-angle excitation.

expression

$$\frac{d\sigma_{\rm qel}}{d\sigma_{\rm Ruth}}(E,\theta_{\rm tel}) = \left[\frac{N_{\rm tel}(E,\theta_{\rm tel})}{N_m(E,\theta_m)}\right]\cdot\left[\frac{(d\sigma_{\rm Ruth}/d\Omega)(E,\theta_m)}{(d\sigma_{\rm Ruth}/d\Omega)(E,\theta_{\rm tel})}\right] \times\left(\frac{\Delta\Omega_m}{\Delta\Omega_{\rm tel}}\right), \quad (3)$$

where $\theta_{\rm tel}(\theta_m)$ is the fixed angle of the telescope (monitor) detector and $N_{\rm tel}(N_m)$ is the corresponding number of detected events of interest in the solid angle $\Delta\theta_{\rm tel}(\Delta\theta_m)$. The $\Delta\Omega_m/\Delta\Omega_{\rm tel}$ ratio was determined bombarding a gold target at low beam energies for which the elastic-scattering cross section follows the Rutherford formula. From measurements of bombarding energies at 14, 17, and 20 MeV, this ratio was estimated to be 0.0534 ± 0.0004 (0.7% statistical uncertainty). It was not required any correction for the angular aperture of the monitors, because they were at a distance of 304 mm from the target and had a circular collimator of 2.5 mm diameter; a correction would be of 0.14%, considered negligible. Figure 1 displays a typical bidimensional spectrum at 24.5 MeV from which events corresponding to $Z = 1$, $Z = 2$, and $Z = 3$ could be detected and separated. Figure 2 shows a

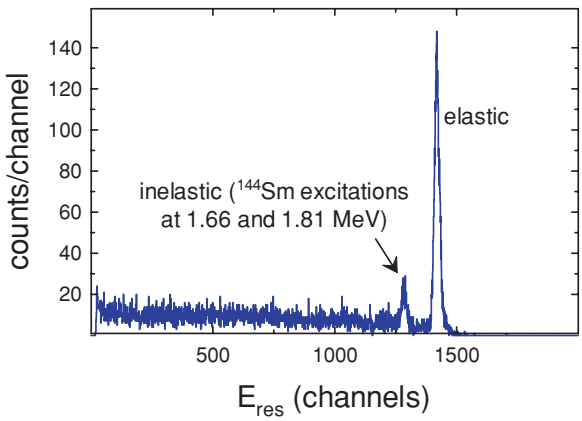

FIG. 2. (Color online) $Z = 3$ projection spectrum on the $E_{\rm res}$ axis for the same system at $E_{\rm lab} = 28.5$ MeV.

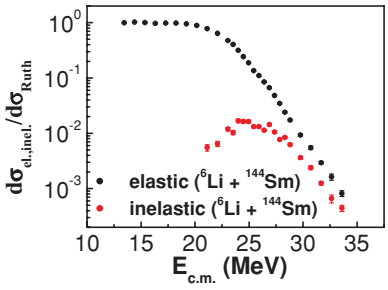

FIG. 3. (Color online) Elastic- and inelastic-scattering excitation functions measured in the present work.

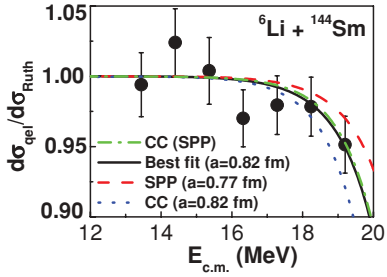

FIG. 4. (Color online) Deep–sub-barrier quasielastic scattering: data and results of the calculations. See text for details.

projection on the residual-energy axis for events with $Z = 3$ events recorded at 28.5 MeV. The peaks corresponding to the elastic-scattering and inelastic scattering excitations of the first two excited states of the ^{144}Sm nucleus (2^+ at 1.66 MeV and 3^- at 1.81 MeV) could be resolved. Events associated with neutron transfer were not observed. Figure 3 shows the elastic and ^{144}Sm inelastic scattering excitation functions measured in the present work.

We did not consider events associated with $Z = 2$ and $Z = 1$ in the analysis of quasielastic processes because we were unable to distinguish clearly their different origins. In fact, those events could come from non–capture breakup, from incomplete fusion reactions, and/or from charged particles evaporation of CF compound nuclei. Therefore, we are not measuring strictly the full quasielastic cross section but rather a lower limit of it, because contributions coming from $Z = 2$ and $Z = 1$ events, associated with NCBU and ICF processes, were not taken into account. For this reason, and in what follows, we will define partial QES as the sum of elastic- and inelastic-scattering channels.

III. PARTIAL QUASIELASTIC SCATTERING AT DEEP–SUB-BARRIER ENERGIES AND THE SURFACE DIFFUSENESS PARAMETER

As it was stated in Sec. I, large-angle quasi-elastic-scattering measurements performed at deep–sub-barrier energies allow one to determine the diffuseness parameter in nucleus-nucleus potentials [12,13]. In this context, the deep–sub-barrier region is usually defined as corresponding to energies lower than around 3 MeV below the lowest barrier height, for which the ratio $d\sigma_{qel}/d\sigma_{Ruth}$ is greater than 0.94 [13]. In this energy region, inelastic excitations and transfer reactions are not expected to play an important role, in which case their couplings should not affect the elastic scattering. Small deviations relative to the Rutherford cross section, which are due to the effect of the nuclear interaction on the QES cross section, can be taken into account by semiclassical perturbation theory and therefore a reliable value for the surface diffuseness of the nuclear potential can be extracted directly.

High precision deep–sub-barrier large-angle QES data have been used to derive the surface diffuseness of interaction potentials of spherical [15–19], deformed [18], and very heavy nuclei [20]. The values obtained for the diffuseness parameter were found to vary in the range from 0.6 to 0.8 fm, compatible with the widely accepted value of $a = 0.63$ fm obtained from systematic analyses of elastic-scattering data [21,22]. So far, this method has not been used with weakly bound nuclei like the ^{6}Li projectile.

To examine the behavior of the diffuseness parameter in the case of a reaction system with a weakly bound projectile following the usual procedure [13], we have compared the data to different calculations. The results are summarized in Fig. 4, which shows the data of QES at deep–sub-barrier energies and theoretical calculations using the code FRESCO [23]. As a bare potential we used the parameter-free double-folding São Paulo potential (SPP) [24,25], which has been able to account for cross sections of different reaction mechanisms in a wide energy range for several systems [26,27], including those involving weakly bound projectiles [28]. To derive the surface diffuseness, a Woods-Saxon (WS) potential equivalent to the SPP at the barrier radius region [24] was actually used as the real potential. This WS equivalent potential was obtained by fitting the SPP at the barrier energy region. The values of the parameters of this potential are $V_0 = 318$ MeV, $r_0 = 0.993$ fm, $a = 0.77$ fm. An imaginary potential was kept well inside the Coulomb barrier to take into account for a small absorption (fusion) through barrier penetration. This inner imaginary potential has a negligible strength in the surface region and consequently the QES cross sections are not sensitive to its parameters. The red (dashed) curve in Fig. 4 is the prediction obtained from optical model calculations without any couplings. The black (full) curve is the result of noncoupled calculations to fit the data taking the surface diffuseness as the only free parameter (a value of 0.82 fm was obtained in this case). We also analyzed the results predicted by coupled-channels calculations in the present system. For example, when one couples the first two excited states of the ^{144}Sm nucleus ($E^* = 1.66$ MeV, 2^+, $\beta_2 = 0.087$ [29] and $E^* = 1.81$ MeV, 3^-, $\beta_3 = 0.13$ [30]), the results do not differ too much from the uncoupled results, as expected for this nearly spherical nucleus. However, when the 3^+ resonant state of the ^{6}Li projectile at 2.18 MeV and $\beta_3 = 0.87$ for $r_0 = 1.06$ fm [4] is included in the coupling scheme, the results change significantly. The blue (dotted) curve shows that the $a = 0.82$ fm value of the diffuseness derived from the best fit of the noncoupling calculations is far from the data when the above coupled-channels scheme is used. However, the green (dashed-dotted) curve is the result of CC calculation using the default value of the SPP, $a = 0.77$ fm. The agreement

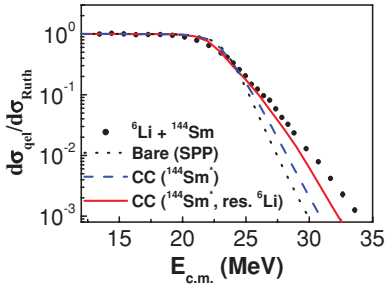

FIG. 5. (Color online) Partial quasi-elastic-scattering excitation function. The curves are results of coupled-channels calculations. See text for details.

between standard SPP estimates (with $a = 0.77$ fm) and experimental results is very good and it is supported by the corresponding χ^2/N values. The fact that channel coupling has a non-negligible effect on the quasielastic scattering even at deep–sub-barrier energies was observed previously [18] for highly deformed systems. In our present calculations we observe that the coupling of sequential breakup of ^{6}Li ($\beta_3 = 0.87$) is also important at deep–sub-barrier energies, a region at which the breakup process is still important.

IV. EXCITATION FUNCTIONS AND BARRIER DISTRIBUTIONS

A. Partial quasielastic scattering

Figure 5 shows the partial QES excitation functions measured in this work. As it was defined in Sec. II, these partial QES cross sections correspond to the sum of elastic and inelastic processes and, consequently, a direct association to CF cannot be done. As bare potential we used the SPP. The curves are predictions from calculations with this bare potential, with no fit search. The black (dotted) curve represents the calculations with no coupling, the blue (dashed) curve is the result when inelastic excitations of the ^{144}Sm nucleus are considered in the coupling scheme performed with the code FRESCO, and the red (full) curve indicates where the ^{6}Li resonant state is also included in the estimates. Although the coupling of the ^{6}Li resonant state, corresponding to the sequential breakup, improves significantly the agreement with the data, the fit is still poor at center-of-mass (c.m.) energies above 25 MeV. An additional coupling of the direct

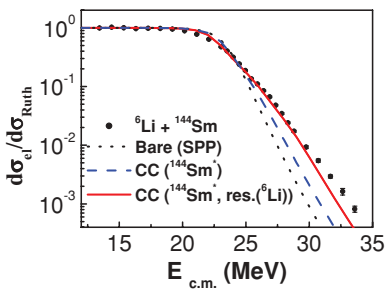

FIG. 6. (Color online) Barrier distribution derived from partial quasielastic scattering. The curves are results of coupled-channels calculations. See text for details.

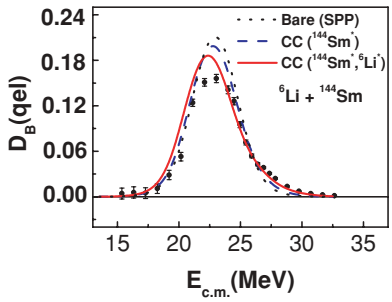

FIG. 7. (Color online) Elastic-scattering excitation function. The curves are results of coupled-channels calculations. See text for details.

breakup channel, not considered in the present calculations, might improve this fit. Figure 6 shows the partial QES barrier distribution derived from the experimental partial QES data, by using a least-squares linear fit method [31] with energy steps of 2 MeV. The $E_{c.m.}$ energies were corrected by the centrifugal potential at 170°, as suggested by Timmers [6]. The curves are theoretical results using the same procedure that was applied to the excitation function. The black (dotted) curve represents the results of the calculations with no coupling, the blue (dashed) curve indicates where the first two inelastic excitations of the ^{144}Sm nucleus are considered in the coupling scheme, and the red (full) curve is the estimate obtained by adding the coupling of the ^{6}Li resonant state. As expected, the coupling of the target nucleus excited states decreases the value of the fusion barrier slightly. Again, as observed with the excitation function, the coupling of the ^{6}Li resonant state improves the agreement with the data. The position of the main barrier does not vary substantially, but the maximum height of the barrier distribution curve decreases. This fact is accompanied by an increment of the curve at higher energies. With the ^{6}Li resonant state coupling, the agreement with the experimental barrier distribution is better, despite of the height of the curve, which might be attributed to the ^{6}Li direct breakup.

B. Elastic scattering

The elastic scattering is related to the total reaction cross section. Therefore, the analysis of the backward-angle elastic barrier distribution should be sensitive to channel couplings and to the reaction barrier structure [10]. Figures 7 and 8

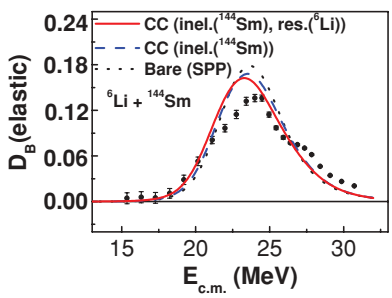

FIG. 8. (Color online) Barrier distribution deduced from elastic scattering. The curves are results of coupled-channels calculations. See text for details.

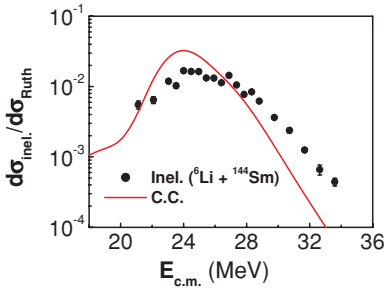

FIG. 9. (Color online) Inelastic-scattering excitation function for the two first excited states of the target. The curves are results of coupled-channels calculations. See text for details.

show the elastic excitation function measured in this work and the corresponding derived barrier distribution, as defined by Eq. (2) in Sec. I. The method to obtain this experimental barrier distribution was similar to the one described for the determination of the barrier distributions from partial backward-angle QES excitation function. The convention used for the curves in the Figs. 7 and 8 is the same as for Figs. 5 and 6. One can observe in these two figures that the coupling of the ^{6}Li resonant state gives a better agreement with both the experimental elastic-scattering excitation function and its associated barrier distribution. However, the results are far from being a reasonable good agreement, particularly in the case of the representation of the barrier distribution. This lack of agreement might be due to the absence of the direct ^{6}Li breakup channel in the coupling scheme. However, as it was remarked in Ref. [10], one has to keep in mind that the structure of this barrier distribution might be inhibited by the presence of weakly coupled channels. As illustration, we also show in Fig. 9 the results of the coupled-channels calculations for the excitation function of the first two excitations of the target inelastic scattering. As there is no fit search, one can observe a reasonable agreement, compatible with what we got for the elastic-scattering excitation function.

V. SUMMARY AND CONCLUSIONS

We obtained high-precision data of elastic and partial quasielastic scattering for the weakly bound ^{6}Li projectile on a ^{144}Sm target at deep–sub-barrier and near- and above-barrier energies. The surface diffuseness of the nuclear interacting potential predicted by the double-folding São Paulo potential was in agreement with our deep–sub-barrier data. As it happens for very deformed systems, the deep–sub-barrier quasielastic scattering of weakly bound systems is affected by coupling effects, being the resonant state of the ^{6}Li, corresponding to the sequential breakup channel, one of the most important couplings to be considered. This channel also significantly bears on the elastic and partial quasielastic excitation functions and their associated barrier distributions at near-barrier energies. Other reaction channels not included in our coupled-channels calculations (like direct breakup) might be needed for full agreement between experimental data and theoretical estimations.

ACKNOWLEDGMENTS

The authors thank CNPq, FAPERJ, CAPES-SECYT, and PROSUL.

[1] L. F. Canto, P. R. S. Gomes, R. Donangelo, and M. S. Hussein, Phys. Rep. **424**, 1 (2006).
[2] M. Dasgupta *et al.*, Phys. Rev. Lett. **82**, 1395 (1999).
[3] M. Dasgupta *et al.*, Phys. Rev. C **66**, 041602(R) (2002).
[4] M. Dasgupta *et al.*, Phys. Rev. C **70**, 024606 (2004).
[5] N. Rowley, G. R. Satchler, and P. H. Stelson, Phys. Lett. **B524**, 25 (1991).
[6] H. Timmers *et al.*, Nucl. Phys. **A584**, 190 (1995).
[7] H. Timmers *et al.*, J. Phys. G **23**, 1175 (1997).
[8] H. Timmers *et al.*, Nucl. Phys. **A633**, 421 (1998).
[9] R. F. Simões *et al.*, Phys. Lett. **B527**, 187 (2002).
[10] N. Rowley *et al.*, Phys. Lett. **B373**, 23 (1996).
[11] C. J. Lin *et al.*, Nucl. Phys. **A787**, 281c (2007).
[12] K. Hagino, T. Takehi, A. B. Balantekin, and N. Takigawa, Phys. Rev. C **71**, 044612 (2005).
[13] K. Washiyama, K. Hagino, and M. Dasgupta, Phys. Rev. C **73**, 034607 (2006).
[14] R. H. Spear, D. C. Kean, M. T. Esat, A. M. R. Joye, and M. P. Fewell, Nucl. Instrum. Methods **147**, 455 (1977).
[15] O. A. Capurro, J. O. Fernández Niello, A. J. Pacheco, and P. R. S. Gomes, Phys. Rev. C **75**, 047601 (2007).
[16] D. S. Monteiro, J. M. B. Shorto, J. F. P. Huiza, P. R. S. Gomes, and E. Crema, Phys. Rev. C **76**, 027601 (2007).
[17] J. F. P. Huiza, E. Crema, D. S. Monteiro, J. M. B. Shorto, R. F. Simoes, N. Added, and P. R. S. Gomes, Phys. Rev. C **75**, 064601 (2007).
[18] L. R. Gasques *et al.*, Phys. Rev. C **76**, 024612 (2007).
[19] H. M. Jia *et al.*, Chin. Phys. Lett. **25**, 2834 (2008).
[20] D. S. Monteiro and P. R. S. Gomes, Phys. Rev. C **77**, 017601 (2008).
[21] P. R. Christnesen *et al.*, Phys. Lett. **B65**, 19 (1976).
[22] C. P. Silva *et al.*, Nucl. Phys. **A679**, 287 (2001).
[23] I. J. Thompson, Comput. Phys. Rep. **7**, 167 (1988) and www.fresco.org.uk.
[24] L. C. Chamon *et al.*, Phys. Rev. C **66**, 014610 (2002).
[25] M. A. G. Alvarez *et al.*, Nucl. Phys. **A723**, 93 (2003).
[26] L. R. Gasques, L. C. Chamon, P. R. S. Gomes, and J. Lubian, Nucl. Phys. **A764**, 135 (2006).
[27] J. J. S. Alves *et al.*, Nucl. Phys. **A748**, 59 (2005).
[28] E. Crema, L. C. Chamon, and P. R. S. Gomes, Phys. Rev. C **72**, 034610 (2005).
[29] S. Raman, C. W. Nestor, Jr., and P. Tikkanen, At. Data Nucl. Data Tables **78**, 1 (2001).
[30] T. Kibedi and R. H. Spear, At. Data Nucl. Data Tables **80**, 35 (2002).
[31] O. A. Capurro *et al.*, Phys. Rev. C **62**, 014613 (2000).